AGU PUBLICATIONS

Geophysical Research Letters

RESEARCH LETTER
10.1002/2016GL067881

Key Points:
- We describe fault evolution over the entire seismic cycle
- We describe fault stability over a wide range of experimental (and natural) conditions
- We account for the diversity of slip events observed at laboratory (and natural) scale

Supporting Information:
- Table S1

Correspondence to:
E. Spagnuolo,
elena.spagnuolo@ingv.it

Citation:
Spagnuolo, E., S. Nielsen, M. Violay, and G. Di Toro (2016), An empirically based steady state friction law and implications for fault stability, *Geophys. Res. Lett.*, *43*, 3263–3271, doi:10.1002/2016GL067881.

Received 20 JAN 2016
Accepted 24 MAR 2016
Accepted article online 30 MAR 2016
Published online 14 APR 2016

An empirically based steady state friction law and implications for fault stability

E. Spagnuolo[1], S. Nielsen[2], M. Violay[3], and G. Di Toro[1,4,5]

[1]Istituto Nazionale di Geofisica e Vulcanologia, Rome, Italy, [2]Department of Earth Sciences, University of Durham, Durham, UK, [3]LEMR, ENAC, École polytechnique fédérale de Lausanne (EPFL), Lausanne, Switzerland, [4]School of Earth, Atmospheric and Environmental Sciences, University of Manchester, Manchester, UK, [5]Dipartimento di Geoscienze, Università degli Studi di Padova, Padua, Italy

Abstract Empirically based rate-and-state friction laws (RSFLs) have been proposed to model the dependence of friction forces with slip and time. The relevance of the RSFL for earthquake mechanics is that few constitutive parameters define critical conditions for fault stability (i.e., critical stiffness and frictional fault behavior). However, the RSFLs were determined from experiments conducted at subseismic slip rates ($V < 1$ cm/s), and their extrapolation to earthquake deformation conditions ($V > 0.1$ m/s) remains questionable on the basis of the experimental evidence of (1) large dynamic weakening and (2) activation of particular fault lubrication processes at seismic slip rates. Here we propose a modified RSFL (MFL) based on the review of a large published and unpublished data set of rock friction experiments performed with different testing machines. The MFL, valid at steady state conditions from subseismic to seismic slip rates (0.1 μm/s $< V <$ 3 m/s), describes the initiation of a substantial velocity weakening in the 1–20 cm/s range resulting in a critical stiffness increase that creates a peak of potential instability in that velocity regime. The MFL leads to a new definition of fault frictional stability with implications for slip event styles and relevance for models of seismic rupture nucleation, propagation, and arrest.

1. Introduction

Friction laws based on one or more state variables are extensively used to model earthquake nucleation, seismic slip, and after slip [*Ruina*, 1980, 1983; *Dieterich*, 1981; *Rice and Ruina*, 1983; *Gu et al.*, 1984; *Okubo and Dieterich*, 1984]. Most friction laws incorporate a dependence on slip history and have the following properties: (1) steady state dependence on velocity, (2) instantaneous dependence on velocity, and (3) evolutionary dependence on characteristic slip distance.

A typical example is the rate-and-state friction law (RSFL) [*Dieterich*, 1978; *Ruina*, 1983] which, in its compact form, can be stated as follows:

$$\mu = \mu_0 + a\ \log(V/V_0) + b\ \log(\theta V_0/D_c) \tag{1}$$

The friction coefficient μ is a function of sliding velocity V and of a state variable θ. The constitutive parameters a, b, and D_c (the characteristic slip distance) are determined by imposing velocity steps (from a fraction of μm/s up to a few cm/s) with respect to a reference slip rate V_0 and friction coefficient μ_0. The θ is often interpreted as an effective average time for the interchange of a population of asperity contacts or a time delay between a change in velocity and the corresponding change in friction coefficient. Its evolution is described by (slowness law [*Dieterich*, 1979]), for example,

$$\mathrm{d}\theta/\mathrm{d}t = 1 - V\theta/\,D_c \tag{2}$$

Once the transient perturbation due to a velocity step is at completion, the steady state friction μ_{ss} is achieved, $\mathrm{d}\theta/\mathrm{d}t = 0$, and $\theta_{ss} = D_c\,/\,V_{ss}$. From equation (1),

$$\mu_{ss} \;=\; \mu_0 + (a-b)\ \log(V/V_0) \tag{3}$$

According to equation (3), depending on the sign of $a - b$, either μ_{ss} increases with increasing slip rate (rate-hardening behavior, resulting in an unconditionally stable behavior) or μ_{ss} decreases with slip rate (rate-weakening behavior, potentially resulting in an unstable behavior leading to dynamic runaway).

The dependency of the steady state friction coefficient on slip rate (equation (3)) also has implications for the stability of a fault in terms of fault stiffness [e.g., *Tse and Rice*, 1986; *Gu and Wong*, 1991]. The steady state condition allows defining a critical stiffness:

Table 1. Best Fit Parameters ($a-b$, V_c, and p) Resulting From Equation (5) (MFL, Figure 2) for a Given Range of σ_n, V_{ss}, and Lithology[a]

Family	Rock Type	Reference[b]	V_{ss} (m s^{-1})	σ_n (MPa)	$a-b$	V_c (m s^{-1})	p
Quartz rich	Sandstone Novaculite	*Di Toro et al.* [2004, 2006 also unpublished data]	1E−10 ÷ 6.5	5 ÷ 18.7	−0.013 ÷ 0.002	0.016 ÷ 0.04	0.42 ÷ 0.86
Carbonate bearing	Calcite	This study, *Han et al.* [2007, 2010], *Shimamoto and Logan* [1981], *Morrow et al.* [2000] and also Di Toro et al. unpublished data	1E−7 ÷ 6.5	5 ÷ 200	−0.0007 ÷ 0.01	0.06 ÷ 0.12	0.78 ÷ 1.07
	Dolomite	This study, *Shimamoto and Logan* [1981], and *Weeks and Tullis* [1985]					
Silicate bearing	Gabbro	*Niemeijer et al.* [2011], *Nielsen et al.* [2008], and *Marone and Cox* [1994]	3E−8 ÷ 6.5	0.5 ÷ 75	0.009 ÷ 0.035	0.02 ÷ 0.093	0.44 ÷ 0.64
	Tonalite	*Di Toro et al.* [2004, 2006, also unpublished data]					
	Monzodiorite	*Mizoguchi and Fukuyama*, [2010]					
	Peridotite	*Del Gaudio et al.* [2009]					
	Granite	*Dieterich* [1978] and *Di Toro et al.* [2004, 2006]					

[a] $V_0 = 1$ μm/s; $\mu_0 = \mu$ (V_0).
[b] When not original, data reported in Figure 2 are from the following sources (see also Table S1).

$$k_c = -\sigma_n V / D_c (\mathrm{d}\mu_{ss}/\mathrm{d}V + F(V, \theta_f)) \quad (4)$$

where σ_n is the effective stress normal to the fault and $F(V, \theta_f)$ is a generic term for inertia at a given state θ_f [*Rice and Ruina*, 1983; *Ruina*, 1983]. Under the assumption of negligible inertia (i.e., quasi-static approximation) equations (3) and (4) yield $k_c = (b-a)\sigma_n/D_c$. The ratio of the stiffness of the system k (either the natural fault plus the wall rocks or the experimental fault plus the apparatus) to k_c determines whether sliding is stable or unstable. For $k > k_c$, the system is stable but can become conditionally stable if perturbed sufficiently [*Gu et al.*, 1984]; if $k < k_c$, sliding is always unstable. Variations in the condition of stability ($k > k_c$) may be induced if any of the constitutive parameters in equation (4) changes, i.e., the dependency of friction coefficient upon slip rate, a situation which is observed within the sliding velocity range discussed here. Experiments performed over a wide range of slip rates have shown that values of μ_{ss} have a pronounced drop for $V > 0.1$ m/s [*Di Toro et al.*, 2011; *Goldsby and Tullis*, 2011]. This drop corresponds to the onset of a dramatic velocity-weakening dependence, with the consequence of substantially increasing k_c in equation (4) and potentially favoring the onset of unstable sliding (see section 4.2). Thus, equations (3) and (4) hold at subseismic velocities, but their validity is questionable at velocities approaching or exceeding a critical velocity $V_c \sim 0.1$ m/s.

Here to shed light onto the change of frictional regime which occurs at the transition from subseismic to seismic slip conditions, we investigate a large data set of published and unpublished data of friction experiments performed with rotary shear, biaxial and triaxial testing machines on silicate-bearing, carbonate-bearing, and quartz-rich rocks (Table 1 and supporting information Table S1). Our aim is to define a μ_{ss} curve whose range of validity extends from subseismic ($V \lesssim 0.1$ m/s) to seismic slip rates ($V \gtrsim 0.1$ m/s) and discuss its implications for fault stability.

2. Methods

We conducted experiments with the rotary shear apparatus SHIVA (Slow to High Velocity Apparatus), which imposes slip rates up to 6.5 m/s and normal stresses up to 40 MPa on solid rock samples with 30/50 mm internal/external diameter [*Di Toro et al.*, 2010; *Niemeijer et al.*, 2011]. We performed experiments with single (Figure 1a) and multiple velocity steps (Figure 1b) on silicate-bearing (microgabbro) and calcite-bearing (Carrara marble, 99% calcite) rocks. Samples were mounted inside an aluminum jacket, embedded within resin, and their surface rectified with a lathe [*Nielsen et al.*, 2012]. The maximum height of the initial surface roughness was less than 10 μm for both rocks. The sample preparation procedure and the stiffness of SHIVA ($k = 0.074$ MPa/μm) resulted in a thorough reproducibility of the experimental data (Figure 1a).

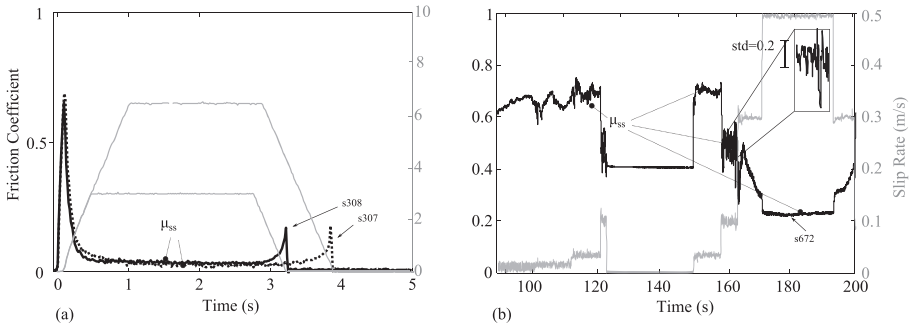

Figure 1. Evolution of friction coefficient with slip and slip rate in experiments performed with SHIVA: (a) velocity control at seismic slip rates (Carrara marble, s308 and s307) and (b) velocity stepping in the intermediate velocity regime (microgabbro, s672) with typical pronounced oscillations of the friction coefficient at $V = 0.1$ m/s. Here the average value of the steady state friction coefficient was determined in the last 50% of cumulated slip resulting in a standard deviation $\Delta\mu_{ss} = 0.2$.

We measured the steady state friction coefficient at a constant velocity as depicted in Figure 1. Experiments are summarized in Table S1 together with data derived from a review of either published or unpublished data sets. The entire data set is synthetized in Table 1 with reference list.

3. Results

We studied the velocity dependence of μ_{ss} and grouped the investigated lithologies under three rock categories (Tables 1 and S1): quartz-rich rocks (novaculite and sandstone), silicate-bearing rocks (microgabbro, monzodiorite, granite, and peridotite), and carbonate-bearing rocks (calcite and dolomite). The frictional response to a velocity step varies slightly with rock category but preserves similar features (Figure 2). Within the entire velocity spectrum it is possible to distinguish three regimes for frictional sliding:

1. Low velocity ($V < 10^{-4}$m/s): μ_{ss} has a log linear dependence with V_{ss} compatible with the RSFL (equation (3)) with $a - b > 0$ (velocity hardening) for silicate-bearing rocks, $a - b < 0$ (velocity weakening) for quartz-rich rocks, and $a - b \sim 0$ (velocity-neutral) for carbonate-bearing rocks.

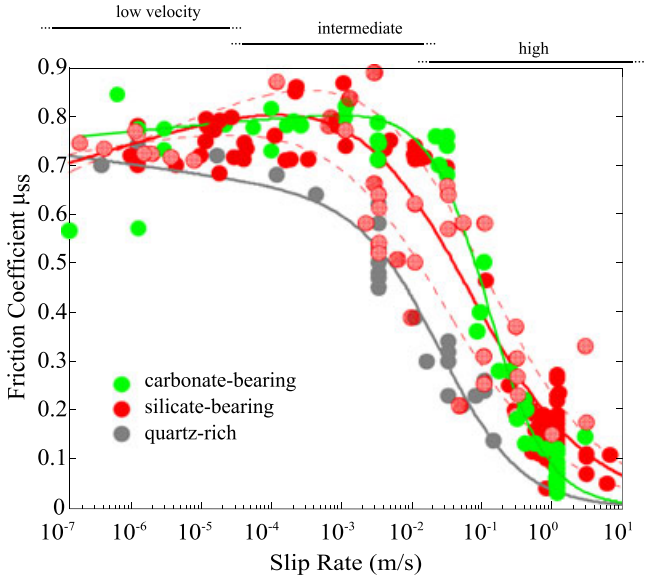

Figure 2. The MFL fit of experimental data under room humidity conditions for the three main rock categories: quartz-rich, silicate-bearing, and carbonate-bearing rocks. Within the silicate-bearing rocks cathegory (red dots) granites are in chess pattern and monzodiorites in stripes. Within the silicate-bearing rocks cathegory (red dots) granites are in chess pattern and monzodiorites in stripes. Each rock category is pertinent to a specific fault lubrication style (see section 4). Experimental data and best fit parameters used in the MFL for each individual lubrication style are listed in Table 1. Given the data scattering for silicate-bearing rocks in the intermediate velocity range (Figure 1b), the 95% interval of confidence is reported for completeness (dashed red lines).

2. Intermediate velocity ($10^{-4} < V \lesssim 10^{-2}$ m/s): the dependence of μ_{ss} with V is negligible in case of silicate- and carbonate-bearing rocks. However, in the experiments performed with SHIVA, this velocity range is associated to the onset of pronounced oscillations around a steady state value (Figure 1b). The amplitude of the oscillations $\Delta\mu$ (~0.2, e.g., Figure 1b) dampens down after either an increase toward seismic slip rates ($V > 10^{-2}$ m/s) or a decrease to subseismic ones ($V < 10^{-4}$ m/s). The $\Delta\mu$ is smaller than the one measured in experiments performed in the same velocity range on monzodiorite (e.g., $\Delta\mu \sim 0.5$ [*Mizoguchi and Fukuyama*, 2010]), probably because of the higher stiffness of SHIVA.
3. High velocity ($V \gtrsim 10^{-2}$ m/s): strong and negative velocity dependence of μ_{ss} in all rock categories.

The velocity dependence of μ_{ss} within the three regimes can be described by a nonlinear least squares empirical fit which results in a modified (rate-and-state) friction law (modified RSFL (MFL), solid curves in Figure 2):

$$\mu_{ss} = [\mu_0 + (a - b)\ \log(V/V_0)] \,/\, (1 + (V/V_c)^p) \tag{5}$$

where $V_0 = 1$ μm /s and μ_0 (V_0) ≈ 0.7 are reference values often used in the RSFL literature. Parameters V_c and p were determined with a best fit procedure resulting in the range of variability reported in Table 1. The $a - b$ value was estimated from the evolution of μ_{ss} in the μ_{ss}-log V plane, i.e., $a - b = \Delta\mu_{ss} / \Delta\log(V_{ss})$. The best fit parameters resulting from equation (5) will be discussed in the next section.

The data scattering for silicate-bearing rocks was large. The standard deviation is shown in Figure 1 for the experiment performed with SHIVA in the intermediate velocity regime but was not available for a large number of the published experiments. We account for the large data scattering of the silicate-bearing rocks category by relaxing the best fit constrains to the 95% interval of confidence (dashed red lines in Figure 2).

4. Discussion

4.1. Rate-Dependent Steady State Curve

The best fit model (MFL) of the entire data set indicates the existence of three velocity-dependent frictional regimes with similar characteristics within each rock category. A critical velocity V_c exists that determines the transition from the intermediate to the high-velocity frictional regime, which is likely dependent on material properties [*Dieterich and Linker*, 1992], as indicated by the variability of V_c with lithology (Table 1). The decay of μ_{ss} with increasing slip rate in the high-velocity regime ($V > V_c$) is described by the parameter p ranging from 0.4 to 1.1 depending on rock category. The two parameters, within each rock category, have a correspondence with the most accredited weakening mechanism operating at seismic velocities in the experiments (see *Niemeijer et al*. [2012] for a review). For cohesive silicate-bearing rocks (microgabbro, granite, tonalite, peridotite, etc.), weakening is promoted by frictional melts which are produced easily at seismic slip rates [e.g., *Tsutsumi and Shimamoto*, 1997; *Di Toro et al*., 2004, 2006, 2011; *Spray*, 2005; *Hirose and Shimamoto*, 2005]. Theoretical interpretation of lubrication operated by friction melts predicts $p \sim 0.5$ [*Nielsen et al*., 2008, 2010], in agreement with the data presented here. Interestingly, V_c ranges from 1 to 9 cm/s in equation (5) to fit the experimental data for silicate-bearing rocks. The estimated V_c is consistent with the critical velocities for the activation of flash heating and melting [*Goldsby and Tullis*, 2002, 2011; *Violay et al*., 2014] due to thermal softening at the asperity scale [see also *Carlson and Langer*, 1989; *Rice*, 2006; *Tullis and Goldsby*, 2003; *Rempel*, 2006; *Beeler et al*., 2008]. For quartz-rich rocks (novaculite) in the absence of melting, fault lubrication has been associated to the amorphization and hydration of quartz in the presence of room humidity at the highly stressed contacts where strained Si-O-Si bonds are highly reactive (silica gel lubrication [*Goldsby and Tullis*, 2002; *Di Toro et al*., 2004; *Nakamura et al*., 2012; *Kirkpatrick et al*., 2013]). Hydrated amorphous silica was found on the slip surface of experimental faults of single crystals and polycrystalline quartz sheared at $V > 3$ mm/s [*Hayashi and Tsutsumi*, 2010; *Nakamura et al*., 2012]. This velocity is almost in the range of the V_c reported in Table 1. For carbonate-bearing rocks weakening has been associated with decarbonation, carbon amorphization, and thermally activated grain size-dependent processes [*Han et al*., 2007, 2010; *Verberne et al*., 2014; *De Paola et al*., 2015; *Green et al*., 2015; *Spagnuolo et al*., 2015]. Also, for this rock category, V_c (ranging from 8 to 13 cm/s) is compatible with the critical slip rate measured in experiments performed on calcitic marbles and limestones [e.g., *Tisato et al*., 2012]. For these rocks, the critical velocity has been interpreted in the framework of the fast-moving dislocation theory [*Spagnuolo et al*., 2015].

The friction coefficient data of silicate-built rocks (e.g., granite and gabbro) are highly scattered due to the following:

1. Mechanical properties of their forming minerals and respective melts (i.e., fracture toughness, melting temperature, and melt viscosity [*Spray*, 1993, 2010]).
2. The nonlinear dependence of shear stress with normal load leading to a nonconstant friction coefficient over the range of normal loads considered here (0.5 to 75 MPa). This is the case for frictional melt lubrication, where the shear stress has a power law dependency on normal stress with an exponent ranging from 0.25 to 0.5 [*Nielsen et al*., 2008; *Niemeijer et al*., 2011; *Violay et al*., 2014].
3. The dependence of the friction coefficient on slip. In Figure 2, we included all the friction data independently of the cumulated slip. However, for rough surfaces of gabbro, *Marone and Cox* [1994] reported $\mu = 0.45$ at slip rates ranging from 1 to 10 μm s^{-1} after a slip < 50 mm and $\mu = 0.7$ after cumulative slip of 53 mm.

Overall, the empirical steady state friction law equation (5), tested over a large data set with different rocks and machines, satisfies the theoretical prediction of an enhanced velocity-weakening condition which was introduced for dynamic fracture simulations [*Zheng and Rice*, 1998] and in models of seismic rupture propagation [e.g., *Noda et al*., 2009, *Dunham et al*., 2011] by setting $p = 1$.

4.2. Frictional Stability and Critical Stiffness Under Variable Rate Dependence

The role of the stiffness in the dynamics of systems controlled by friction has been extensively discussed in theoretical and numerical studies [e.g., *Dieterich*, 1979; *Rice and Ruina*, 1983; *Putelat et al*., 2011; *Belardinelli and Belardinelli*, 1996; *Tse and Rice*, 1986; *Gu and Wong*, 1991]. The fault + wall rock system was described by spring-slider models where a sliding mass is loaded through a spring by a driver moving at constant velocity V_{ss}. The frictional instability is triggered if $d\mu_{ss} / dV < 0$ and $k \leq k_c$, where k_c is the critical stiffness of the apparatus or of the wall rocks in nature [*Rice and Ruina*, 1983]. The k_c is defined in equation (4) under the quasi-static approximation which implies that velocity is the fastest evolving variable of the system and it responds instantaneously (negligible inertia) to a variation of the boundary conditions [*Gu et al*., 1984; *Belardinelli and Belardinelli*, 1996]. Assuming that the quasi-static approximation holds, we compute k_c according to equation (5) for V ranging from subseismic to seismic slip rates for $\sigma_n = 10$ MPa and $D_c = 1$ μm, 10 μm, and 100 μm. The k_c (V) is plotted in Figure 3a together with the machine stiffness of SHIVA ($k = 0.074$ MPa/μm) and of other machines (0.1 MPa/μm [*Byerlee and Brace*, 1968], 0.04 MPa/μm [*Dieterich*, 1979], and 0.105 MPa/μm [*Marone et al*., 1990]). For silicate- and carbonate-bearing rocks given a typical laboratory $D_c \sim 1$ μm k_c (V) intersects the machines stiffness in the gray shaded area at $V \sim 10^{-4}$–10^{-3} m/s, switching the experimental fault + machine system from stable ($k_c < k$) to unstable ($k_c > k$) sliding. As velocity further increases and once the intermediate velocity regime is overcome, $d\mu_{ss}/dV$ begins to wane and k_c decreases until eventually $k_c < k$ so that the system returns to a condition of stability in the high-velocity regime. We note that at high velocity the inertial terms may cease to be negligible [*Baumberger et al*., 1994]. In this regime, the inertial terms are essentially stabilizing, provided that both $d\mu_{ss}/dV$ and $\partial\mu/\partial V$ are negative, which is what we observe experimentally at high velocities. If the critical stiffness is less but close to the stiffness of the apparatus (intermediate velocity regime), permanently sustained oscillations occur as observed for the example in Figure 1b and previous experiments [e.g., *Tullis and Weeks*, 1986; *Mizoguchi and Fukuyama*, 2010], in agreement with theoretical linearized stability analysis [e.g., *Gu et al*., 1984].

In general, from Figure 3a, given a D_c value, the intersection between k_c and k indicates the velocity regime where frictional instability can occur. Conversely, given a value for stiffness, $a - b$, and a velocity regime where oscillations occur, it is possible to determine an approximate value for D_c. However, D_c is not necessarily constant in the three velocity regimes; thus, the estimated D_c is the ultimate value prior to the onset of the frictional oscillations. In Figure 3a each k_c curve represents one stability status of the system given an initial population of asperities whose renewal requires a distance D_c. If D_c increases with velocity (or slip) the intersection between the k_c and k curves shifts toward higher velocities.

The evolution of effective k_c throughout the slip velocity spectrum, as described above, has a number of implications for fault stability. For example, it can explain why the realization of friction experiments at either high (~1 m/s or more) or low (<1 cm/s) velocity is less challenging than at intermediate velocity. Indeed, at intermediate velocity the stability, and hence control of the system, are more difficult to achieve due to

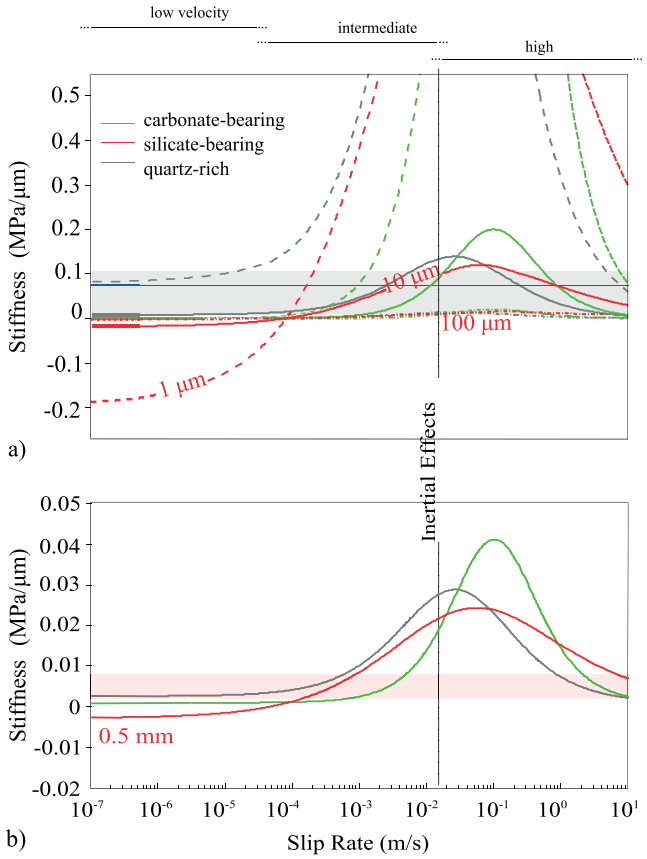

Figure 3. The critical stiffness k_c from equation (4) versus machine (or natural) stiffness k for the three rock categories. (a) Laboratory faults: k_c is computed using the MFL (equation (5)) for $\sigma_n = 10$ MPa. Dashed, solid, and dash-dotted lines are for $D_c = 1$ μm, 10 μm, and 100 μm, respectively. The $k = 0.074$ MPa/μm for SHIVA is in blue solid line; a range of other machine stiffness corresponds to the gray shaded area. For $k_c < k$ frictional sliding is stable; for $k_c \approx k$ and $V \sim 0.1$ m/s (intermediate velocity regime) theoretical stability analysis predicts the onset of oscillations, consistently with experimental observations (Figure 1b). For $k_c > k$ ($V > V_c$) the friction coefficient drops, and inertial effect may become dominant. (b) Natural faults: k_c results from the extrapolation of the MFL to natural conditions ($\sigma_n = 100$ MPa, $D_c = 0.5$ mm). A range of k for natural faults (red shaded area) was computed assuming a fault patch radius between 5 and 50 m and shear stiffness of $G = 25$ GPa.

the peak in k_c (Figure 1b). In addition, the velocity dependence of k_c indicates that variability in slip patterns (stable sliding, slow slip pulses, and stick slip) can be expected on a given fault, as observed in the experiments here, and will possibly contribute to the variety of slip behavior observed on natural faults.

4.3. Implications for Fault Stability

From Figure 3a, when $D_c \geq 100$ μm, k_c curves rarely intersect the machine stiffness zone implying that experimental faults with D_c greater than the upper limit observed in experiments are in a condition of stable slip over the entire velocity spectrum. However, in the case of natural faults, all other variables in equations (4) and (5), and the stiffness of the system should be rescaled. Though the stiffness of natural faults varies sensibly throughout the evolution of the fault zone with repeated slip events [*Griffith et al.*, 2009], a rough estimation for the stiffness right before the earthquake derives from [*Eshelby*, 1957]

$$k = 7\pi G/16r \qquad (6)$$

using the simplest approximation of a buried circular crack of radius r and shear modulus G and assuming that the earthquake instability does not propagate beyond the nucleation patch. We can use indicatively $G = 25$ GPa (e.g., granite) and r ranging from 5 to 50 m resulting in $k = [0.7–7]\ 10^{-3}$ MPa/μm per unit fault area, up to 1 order of magnitude smaller than the stiffness of SHIVA. The conditions of stability for faults can be extrapolated as reported in Figure 3b, computing equation (4) with $\sigma_n = 100$ MPa (approximatively the lithostatic load at 4 km depth) and $D_c = 0.5$ mm. Again, oscillations are expected when k_c is close to k. As a result of the scaling shown in Figure 3 b, it appears that a natural fault patch is not necessarily locked into either stable or unstable conditions. A given fault may evolve within three different regimes, depending on slip velocity. If slip rate gradually increases (for example, under the effect of an increased tectonic load) the fault will first encounter a stable slip episode which will last as long as $k_c < k$ (in Figure 3b, slip rate below 10^{-4} m/s for the case where $D_c = 0.5$ mm, red solid curve). As the fault slip accelerates, k_c may increase to a point where it approaches fault stiffness k. Then the fault may respond to small perturbations by oscillations or stick-slip motion, a sign that it is close to instability limit $k_c \sim k$. As the fault accelerates further to $k_c > k$, it may eventually dynamically weaken and enter a seismic transient episode. The above sequence of events may represent a type of precursory pattern, with accelerating slip and moderate seismic unrest preceding an earthquake rupture. We note that in addition to the evolution of k_c described above, another well-known mechanism for the transition from stable to unstable sliding is the growth of the slip patch radius r, with the consequent decrease in k according to equation (6).

5. Conclusions

A modified friction law (MFL, equation (5)) describes the steady state conditions over the entire velocity spectrum where we identify three velocity regimes for frictional behavior. Two parameters describe the three regimes, the critical velocity V_c and the exponent p (Table 1) which are material dependent and likely related to specific physicochemical processes occurring at the asperity scale and within the slipping zone.

First, according to the MFL, critical conditions for laboratory fault stability (k_c and D_c) are not constant but evolve with slip rate, and their evolution can justify slip accelerations on materials expected to slip stably (e.g., $a-b>0$ for silicate-bearing rocks in Figure 3a). Consequently, the parameter $a-b$ alone cannot be intended as a watershed between the unconditionally stable and potentially unstable frictional behaviors. *Noda and Lapusta* [2013] achieved similar conclusions for fault stability using rapid shear heating of pore fluids to combine the stable slip to the fast coseismic weakening.

Second, the MFL describes two possible steady state conditions for a given μ_{ss}, at least in the case of silicate-bearing rocks of the present data set (Figure 2), one in the low-velocity and one in the high-velocity regime. Consequently, experimental faults slipping stably at low velocities can jump into the high-velocity regime under a "velocity kick" [*Scholz*, 1998] that forces the fault to overcome a critical slip or stiffness.

Third, $k_c(V)$ has a pronounced peak at intermediate slip velocities (i.e., $V \sim V_c$) and for $D_c = 10\,\mu$m the estimated k_c is larger than the stiffness of all rotary shears. The k_c peak explains why experiments performed in the intermediate velocity regime are extremely demanding resulting often in sample failure and do require machines with very high stiffness for control purposes. However, at higher velocities ($V > 0.1$ m/s) k_c drops again below the typical machine stiffness, and stable behavior is expected. Consequently, the high-velocity regime represents a state of stable sliding in the sense of perturbation theory, resulting in manageable experimental control.

The scaling of stability conditions to natural faults is discussed under the opportune scaling of stiffness and D_c. In nature, at seismogenic depths (e.g., $\sigma_n = 100$ MPa), oscillations attributed to frictional instabilities are expected to occur in a range of slip rates (10^{-4}–10^{-3} m/s) that is lower than the range (10^{-3}–10^{-2} m/s) of experimental faults. The estimates given here are qualitative because of the strong assumptions made on natural fault stiffness.

Differently from previous theoretical studies the MFL here proposed is based on experiments performed on different rock types with several machines. The MFL predicts a variable critical stiffness that describes the behavior of faults under dynamic loading conditions in association with the occurrence of at least three frictional regimes and slip event styles. Accordingly, under the opportune scaling, the MFL is effective in explaining the plethora of events observed during the seismic cycle and might be applied to both observational seismology and earthquake modeling.

Acknowledgments

We acknowledge funding by the European Research Council project 614705 NOFEAR. We thank Piergiorgio Scarlato for laboratory support, Chris Marone and Terry Tullis for discussions, Ashley Griffith, an anonymous reviewer, and the Editor for their constructive comments. E.S. wrote the first draft of the paper; all authors contributed to concept development, data interpretation, and to the editing of the manuscript. Supporting information is available in the online version of the paper. Correspondence and requests for materials should be addressed to elena.spagnuolo@ingv.it.

References

Baumberger, T., F. Heslot, and B. Perrin (1994), Crossover from creep to inertial motion in friction dynamics, *Nature*, *367*, 544–546.

Beeler, N. E., T. E. Tullis, and D. L. Goldsby (2008), Constitutive relationships and physical basis of fault strength due to flash heating, *J. Geophys. Res.*, *113*, B01401, doi:10.1029/2007JB004988.

Belardinelli, M. E., and E. Belardinelli (1996), The quasi-static approximation of the spring-slider motion, *Nonlinear Process. Geophys.*, *3*, 143–149, doi:10.5194/npg-3-143-1996.

Byerlee, J. D., and W. F. Brace (1968), Stick slip, stable sliding, and earthquakes: Effect of rock type, pressure, strain rate and stiffness, *J. Geophys. Res.*, *73*, 6031–6037, doi:10.1029/JB073i018p06031.

Carlson, J. M., and J. S. Langer (1989), Properties of earthquakes generated by fault dynamics, *Phys. Rev. Lett.*, *62*(22), 2632–2635.

De Paola, N., R. E. Holdsworth, C. Viti, C. Collettini, and R. Bullock (2015), Can grain size sensitive flow lubricate faults during the initial stages of earthquake propagation?, *Earth Planet. Sci. Lett.*, *431*, 48–58.

Del Gaudio, P., G. Di Toro, T. Hirose, S. Nielsen, and T. Shimamoto (2009), Frictional melting of peridotite and seismic slip, *J. Geophys. Res.*, *114*, B06306, doi:10.1029/2008JB005990.

Di Toro, G., D. L. Goldsby, and T. E. Tullis (2004), Friction falls towards zero in quartz rock as slip velocity approaches seismic rates, *Nature*, *427*, 436–439.

Di Toro, G., T. Hirose, S. Nielsen, G. Pennacchioni, and T. Shimamoto (2006), Natural and experimental evidence of melt lubrication of faults during earthquakes, *Science*, *311*, 647–649.

Di Toro, G., et al. (2010), From field geology to earthquake simulation: A new state-of-the-art tool to investigate rock friction during the seismic cycle (SHIVA), *Rend. Fis. Accad. Lincei*, *21*, S95–S114.

Di Toro, G., R. Han, T. Hirose, N. D. Paola, S. Nielsen, K. Mizoguchi, F. Ferri, M. Cocco, and T. Shimamoto (2011), Fault lubrication during earthquakes, *Nature*, *471*, 494.

Dieterich, J. H. (1978), Preseismic fault slip and earthquake prediction, *J. Geophys. Res.*, *83*, 3940–3948, doi:10.1029/JB083iB08p03940.

Dieterich, J. H. (1979), Modelling of rock friction and the mechanism of the stick-slip, *Pure Appl. Geophys.*, *84*, 2161–2168.
Dieterich, J. H. (1981), Constitutive properties of faults with simulated gouge, *Geophys. Monogr. Ser.*, *24*, 103–120, doi:10.1029/GM024p0103.
Dieterich, J. H., and M. F. Linker (1992), Fault stability under conditions of variable normal stress, *Geophys. Res. Lett.*, *19*(16), 1691–1694, doi:10.1029/92GL01821.
Dunham, E. M., D. Belanger, L. Cong, and J. E. Kozdon (2011), Earthquake Ruptures with Strongly Rate-Weakening Friction and Off-Fault Plasticity, Part 1: Planar Faults, *Bull. Seismol. Soc. Am.*, *101*(5), 2296–2307.
Eshelby, J. D. (1957), The determination of the elastic field of an ellipsoidal inclusion and related problems, *Proc. R. Soc. Ser. A*, *241*, 376–396.
Goldsby, D. L., and T. E. Tullis (2002), Low frictional strength of quartz rocks at subseismic slip rate, *Geophys. Res. Lett.*, *29*(17), 1844, doi:10.1029/2002GL015240.
Goldsby, D. L., and T. E. Tullis (2011), Flash heating leads to low frictional strength of crustal rocks at earthquake slip rates, *Science*, *334*(6053), 216–218, doi:10.1126/science.1207902.
Green, H. W., F. Shi, K. Bozhilov, G. Xia, and Z. Reches (2015), Phase transformation and nanometric flow cause extreme weakening during fault slip, *Nat. Geosci.*, doi:10.1038/NGEO2436.
Griffith, W. A., P. F. Sanz, and D. Pollard (2009), Influence of outcrop scale fractures on the effective stiffness of fault damage zone rocks, *Pure Appl. Geophys.*, *166*, 1595–1627.
Gu, J.-C., J. J. R. Rice, A. L. Ruina, and S. T. Tse (1984), Slip motion and stability of a single degree of freedom elastic system with rate and state dependent friction, *J. Mech. Phys. Solids*, *32*(3), 167–196.
Gu, Y., and T. F. Wong (1991), Effects of loading velocity, stiffness and inertia on the dynamics of a single degree of freedom spring-slider system, *J. Geophys. Res.*, *96*, 21,667–21,691, doi:10.1029/91JB02271.
Han, R., T. Shimamoto, J. I. Ando, and J.-H. Ree (2007), Seismic slip record in carbonate-bearing fault zones: An insight from high velocity friction experiments on siderite gouge, *Geology*, *35*, 1131–1134.
Han, R., T. Hirose, and T. Shimamoto (2010), Strong velocity weakening and powder lubrication of simulated carbonate faults at seismic slip rates, *J. Geophys. Res.*, *115*, B03412, doi:10.1029/2008JB006136.
Hayashi, N., and A. Tsutsumi (2010), Deformation textures and mechanical behavior of a hydrated amorphous silica formed along an experimentally produced fault in chert, *Geophys. Res. Lett.*, *37*, L12305, doi:10.1029/2010GL042943.
Hirose, T., and T. Shimamoto (2005), Growth of molten zone as a mechanism of slip weakening of simulated faults in gabbro during frictional melting, *J. Geophys. Res.*, *110*, B05202, doi:10.1029/2004JB003207.
Kirkpatrick, J. D., C. D. Rowe, J. C. White, and E. E. Brodsky (2013), Silica gel formation during fault slip: Evidence from the rock record, *Geology*, *41*(9), 1015–1018.
Marone, C., and S. J. D. Cox (1994), Scaling of rock friction constitutive parameters: The effects of surface roughness and cumulative offset on friction of gabbro, *Pure Appl. Geophys.*, *143*, 359–385.
Marone, C., C. B. Raleigh, and C. H. Scholz (1990), Frictional behavior and constitutive modelling of simulated fault gouge, *J. Geophys. Res.*, *95*, 7007–7025, doi:10.1029/JB095iB05p07007.
Mizoguchi, K., and E. Fukuyama (2010), Laboratory measurements of rock friction at subseismic slip velocities, *Int. J. Rock Mech. Min. Sci.*, *47*, 1363–1371, doi:10.1016/j.ijrmms.2010.08.013.
Morrow, C. A., D. E. Moore, and D. A. Lockner (2000), The effect of mineral bond strength and adsorbed water on fault gouge frictional stregnth, *Geophys. Res. Lett.*, *27*(6), 815–818.
Nakamura, Y., J. Muto, H. Nagahama, I. Shimizu, T. Miura, and I. Arakawa (2012), Amorphization of quartz by friction: Implication to silica-gel lubrication of fault surfaces, *Geophys. Res. Lett.*, *39*, L21303, doi:10.1029/2012GL053228.
Nielsen, S. B., E. Spagnuolo, and M. Violay (2012), The ultimate sample preparation for rotary shear experiments Rapporti Tecnici INGV, (215).
Nielsen, S., G. D. Toro, T. Hirose, and T. Shimamoto (2008), Frictional melt and seismic slip, *J. Geophys. Res.*, *113*, B01308, doi:10.1029/2007JB005122.
Nielsen, S., P. Mosca, G. Giberti, G. D. Toro, T. Hirose, and T. Shimamoto (2010), On the transient behavior of frictional melt during seismic slip, *J. Geophys. Res.*, *115*, B10301, doi:10.1029/2009JB007020.
Niemeijer, A. R., G. Di Toro, S. Nielsen, and F. D. Felice (2011), Frictional melting of gabbro under extreme experimental conditions of normal stress, acceleration and sliding velocity, *J. Geophys. Res.*, *116*, B07404, doi:10.1029/2010JB008181.
Niemeijer, A. R., G. Di Toro, W. A. Griffith, A. Bistacchi, S. Smith, and S. Nielsen (2012), Inferring earthquake physics and chemistry using an integrated field and laboratory approach, *J. Struct. Geol.*, *39*, 2–36.
Noda, H., and N. Lapusta (2013), Stable creeping fault segments can become destructive as a result of dynamic weakening, *Nature*, *493*, 518–521.
Noda, H., E. M. Dunham, and J. R. Rice (2009), Earthquake ruptures with thermal weakening and the operation of major faults at low overall stress levels, *J. Geophys. Res.*, *114*, B07302, doi:10.1029/2008JB006143.
Okubo, P. G., and J. H. Dieterich (1984), Effects of physical fault properties on frictional instabilities produced on simulated faults, *J. Geophys. Res.*, *89*(B7), 5817–5827.
Putelat, T., J. H. P. Dawes, and J. R. Willis (2011), On the microphysical foundation of rate-and-state friction, *J. Mech. Phys. Solids*, *59*, 1062–1075.
Rempel, A. W. (2006), The effects of flash weakening and damage on the evolution of fault strength and temperature, in *Earthquakes: Radiated Energy and the Physics of Faulting*, vol. 170, pp. 263–270, AGU, Washington, D. C.
Rice, J. R. (2006), Heating and weakening of faults during earthquake slip, *J. Geophys. Res.*, *111*, B05311, doi:10.1029/2005JB004006.
Rice, J. R., and A. L. Ruina (1983), Stability of steady frictional slipping, *J. Appl. Mech.*, *50*, 343–349.
Ruina, A. L. (1980), Friction laws and instabilities: A quasistatic analysis of some dry frictional behaviour, PhD thesis, Brown University.
Ruina, A. L. (1983), Slip instability and state variable friction laws, *J. Geophys. Res.*, *88*, 10,359–10,370, doi:10.1029/JB088iB12p10359.
Scholz, C. H. (1998), Earthquakes and friction laws, *Nature*, *391*, 37–42.
Shimamoto, T., and J. M. Logan (1981), Effects of simulated fault gouge on the sliding behaviour of Tennessee sandstone: Nonclay gouges, *J. Geophys. Res.*, *86*, 2902–2914, doi:10.1016/0040-1951(84)90138-0.
Spagnuolo, E., O. Plümper, M. Violay, A. Cavallo, and G. Di Toro (2015), Fast-moving dislocations trigger flash weakening in carbonate bearing faults during earthquakes, *Sci. Rep.*, *5*, 16112, doi:10.1038/srep16112.
Spray, J. G. (1993), Viscosity determinations of some frictionally generated silicate melts: Implications for fault zone rheology at high strain rates, *J. Geophys. Res.*, *98*(B5), 8053–8068, doi:10.1029/93JB00020.
Spray, J. G. (2005), Evidence for melt lubrication during large earthquakes, *Geophys. Res. Lett.*, *32*, L07301, doi:10.1029/2004GL022293.
Spray, J. G. (2010), Frictional melting processes in planetary materials: From hyper velocity impact to earthquakes, *Annu. Rev. Earth Planet. Sci.*, *38*, 221–254.

Tisato, N., G. Di Toro, N. De Rossi, M. Quaresimin, and T. Candela (2012), Experimental investigation of flash weakening in limestone, *J. Struct. Geol.*, *38*, 183–199, doi:10.1016/j.jsg.2011.11.017.

Tse, S., and J. R. Rice (1986), Crustal earthquake instability in relation to the depth variation of frictional properties, *J. Geophys. Res.*, *91*, 9452–9472, doi:10.1029/JB091iB09p09452.

Tsutsumi, A., and T. Shimamoto (1997), High-velocity frictional properties of gabbro, *Geophys. Res. Lett.*, *24*, 699–702, doi:10.1029/97GL00503.

Tullis, T. E., and D. L. Goldsby (2003), Flash melting of crustal rocks at almost seismic slip rates, *Eos Trans. AGU*, *84*(46), Fall Meet. Suppl., Abstract S51B-05.

Tullis, T. E., and J. D. Weeks (1986), Constitutive behavior and stability of frictional sliding of granite, *PAGEOPH*, *124*, 383–414.

Verberne, B. A., O. Plümper, D. A. M. de Winter, and C. Spiers (2014), Superplastic nanofibrous slip zones control seismogenic fault friction, *Science*, *346*(6215), 1342–1344.

Violay, M., G. Di Toro, B. Gibert, S. Nielsen, E. Spagnuolo, P. Del Gaudio, P. Azais, and P. G. Scarlato (2014), Effect of glass on the frictional behavior of basalts at seismic slip rates, *Geophys. Res. Lett.*, *41*, 348–355, doi:10.1002/2013GL058601.

Weeks, J. D., and T. E. Tullis (1985), Frictional sliding of dolomite: A variation in constitutive behavior, *J. Geophys. Res.*, *90*, 7821–7826, doi:10.1029/JB090iB09p07821.

Zheng, G., and J. R. Rice (1998), Conditions under which velocity weakening friction allows a self-healing versus a crack-like mode of rupture, *Bull. Seismol. Soc. Am.*, *88*(6), 1466–1483.